

# AVA: A Video Dataset of Spatio-temporally Localized Atomic Visual Actions

Chunhui Gu\*    Chen Sun\*    David A. Ross\*    Caroline Pantofaru\*    Yeqing Li\*  
 Sudheendra Vijayanarasimhan\*    George Toderici\*    Susanna Ricco\*    Rahul Sukthankar\*  
 Cordelia Schmid<sup>†</sup>\*    Jitendra Malik<sup>‡</sup>\*

## Abstract

This paper introduces a video dataset of spatio-temporally localized Atomic Visual Actions (AVA). The AVA dataset densely annotates 80 atomic visual actions in 57.6k movie clips with actions localized in space and time, resulting in 210k action labels with multiple labels per human occurring frequently. The main differences with existing video datasets are: (1) the definition of atomic visual actions, which avoids collecting data for each and every complex action; (2) precise spatio-temporal annotations with possibly multiple annotations for each human; (3) the use of diverse, realistic video material (movies). This departs from existing datasets for spatio-temporal action recognition, such as JHMDB and UCF datasets, which provide annotations for at most 24 composite actions, such as basketball dunk, captured in specific environments, i.e., basketball court.

We implement a state-of-the-art approach for action localization. Despite this, the performance on our dataset remains low and underscores the need for developing new approaches for video understanding. The AVA dataset is the first step in this direction, and enables the measurement of performance and progress in realistic scenarios.

## 1. Introduction

This paper introduces a new annotated video dataset, AVA, which we have collected to support research on action recognition. Fig. 1 shows representative frames. The annotation is person-centric. Every person is localized using a bounding box and the attached labels correspond to (possibly, multiple) actions being performed by the person. There is one action corresponding to the **pose of the person** (orange text) — whether he or she is standing, sitting, walking, swimming etc. — and there may be additional actions corresponding to **interactions with objects** or **human-human**

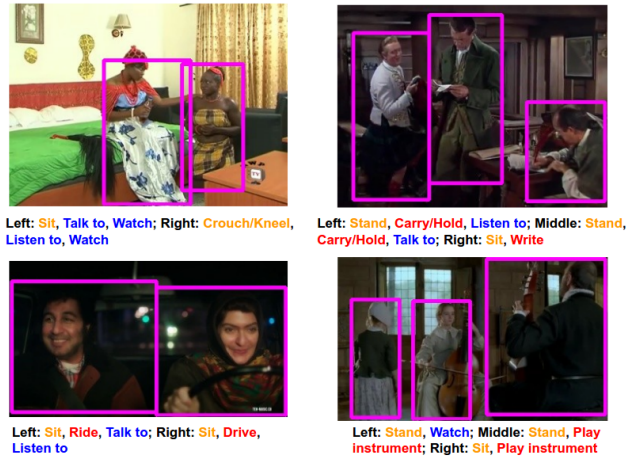


Figure 1. The bounding box and action annotations in sample frames of the AVA dataset. Each bounding box is associated with 1 pose action (in orange), 0–3 interactions with objects (in red), and 0–3 interactions with other people (in blue). Note that some of these actions require temporal context to accurately label.

**interactions** (red or blue text). The proposed framework naturally accommodates different people performing different actions.

Our data source is movies – feature films produced in Hollywood or elsewhere – and we analyze successive 3 second long video segments. In each segment, the middle frame is annotated as described above, but the annotators use perceptual cues available from the larger temporal context of the video, including movement cues. The fine scale of the annotations motivates our calling them “Atomic Visual Actions”, abbreviated as AVA for the name of the dataset. The vocabulary currently consists of 80 different atomic visual actions. Our dataset consists of 57.6k video segments collected from 192 different movies, where segments are 3 second long videos extracted sequentially in 15 minute chunks from each movie. Using chunks of 15 minutes per video enables diversity at the same time as continuity. We labeled a total of 210k actions, demonstrating that multiple action labels occur frequently. We plan to release the dataset of annotations to the computer vision commu-

\*Google Inc., USA

<sup>†</sup>Inria, Laboratoire Jean Kuntzmann, Grenoble, France

<sup>‡</sup>University of California at Berkeley, USA

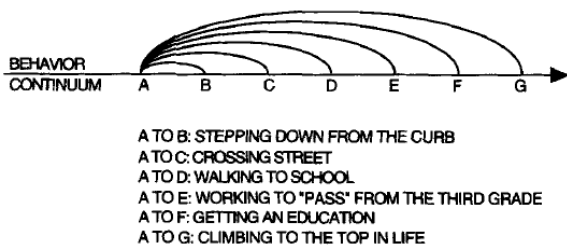


Figure 2. This figure illustrates the hierarchical nature of an activity. From Barker and Wright [3], pg. 247.

nity.

To motivate the design choices behind AVA, we list below some key findings from the human psychology literature on activity and events. We recommend [38] to the reader interested in a more detailed account.

Foundational work [3] observed in meticulous detail the children of a small town in Kansas going about their daily lives. They proposed a unit they called a “behavior episode”. Examples of behavior episodes include a group of boys moving a crate across a pit, a girl exchanging remarks with her mother, and a boy going home from school. They noted the hierarchical nature of activity, illustrated in Fig. 2 [3]. At the finest level the actions can be described as simple body movements or manipulation of objects but at coarser levels the most natural descriptions are in terms of intentionality and goal-directed behavior, as already noted in movies of simple moving geometrical figures where such attribution is common among human observers [14].

Newtonson [24] experimentally studied how humans perceive a videotaped behavior sequence by asking them to use key presses to mark breakpoints between segments. Zacks et al. [39] applied this technique to study how human perceive everyday activities such as making a bed or doing the dishes. There was clear evidence of hierarchical event structure; the large unit boundaries were also likely to be small unit boundaries.

We are now ready to justify three key design choices in AVA:

**Why short temporal scale?** Coarse-scale activity/event understanding is best done in terms of goals and subgoals. But this is essentially an infinite set just like the set of all sentences. Another problem is that goals may not even be evident visually. If we see someone walking, are they doing it for exercise or to get to the grocery store? However if we limit ourselves to fine scales, then the actions are very physical in nature and have clear visual signatures. We hope to eventually understand the coarser scales of activity analysis mediated by conceptual structures such as scripts and schemas, composed from fine scale AVA units, but this is very much future work. Research such as Zachs

et al. [39] shows that coarse scale boundaries are a subset of fine scale boundaries and suggests that the fine scale units should prove useful in composing coarser units. We choose to annotate keyframes in 3 second long video segments, as this is dense enough to understand the content and avoids precise temporal annotation shown to be difficult to define precisely; the THUMOS challenge [16] observed that action boundaries (unlike objects) are vague and subjective, leading to significant inter-annotator disagreement and evaluation bias. By contrast, it is feasible for annotators to determine (using  $\pm 1.5s$  of context) whether a specific frame *contains* the given action. This task is intrinsically less ambiguous than precisely specifying the temporal boundaries.

**Why person-centric?** There are events such as trees falling which do not involve people, but our focus is on the activities of people, treated as single agents. There could be multiple people as in a sports event or just two people hugging, but each one is an agent with his or her own choices, so we can treat each separately. We do not preclude cooperative or competitive behavior, but each agent is described by pose and interaction with objects and humans.

**Why movies?** Ideally we want behavior “in the wild”, recorded in a digital form by a modern day version of Barker and Wright [3]. We do not have that. The next best thing is movies. For more than a hundred years cinematographers have been narrating stories in this medium, and if we consider the variety of genres (thrillers, drama, romantic comedies, westerns etc.) and countries with flourishing movie industries (USA, UK, India, China, Japan, Russia etc.) we may expect a significant range of human behavior to show up in these stories. We expect some bias in this process. Stories have to be interesting (To quote David Lodge: Literature is mostly about having sex and not much about having children. Life is the other way round.) and there is a grammar of the film language [2] that communicates through the juxtaposition of shots. That said, in one shot we expect an unfolding sequence of human actions, somewhat representative of reality, as conveyed by good actors. It is not that we regard this data as perfect, just that it is better than working with the assortment of user generated content such as videos of animal tricks, DIY instructional videos, events such as children’s birthday parties, and the like. We expect movies to contain a greater range of activities as befits the telling of different kinds of stories. We make it a point to only include video from movies which are at least 30 minutes long, sampling 15 minute intervals.

This paper is organized as follows. In Section 2 we review previous action recognition datasets and point out the difference with our AVA dataset. In Section 3, we describe the annotation process. Section 4 presents some interesting statistics from the dataset. Section 5 explains the baseline approach and reports results. We conclude in Section 6.

## 2. Related work

Most popular action recognition datasets, such as KTH [31], Weizmann [4], Hollywood-2 [22], HMDB [21] and UCF101 [33], consist of short clips, manually trimmed to capture a single action. These datasets are ideally suited for training fully-supervised, whole-clip, forced-choice classifiers. Unfortunately, although convenient, this formulation of action recognition is completely unrealistic – real-world action recognition always occurs in an untrimmed video setting and frequently demands spatial grounding as well as temporal localization.

Recently, video classification datasets, such as TrecVid multi-media event detection [25], Sports-1M [19] and YouTube-8M [1], have focused on video classification on a large-scale, in some cases with automatically generated – and hence potentially noisy – annotations. They serve a valuable purpose but address a different need than AVA.

Another line of recent work has moved away from video classification towards temporal localization. ActivityNet [6], THUMOS [16], MultiTHUMOS [36] and Charades [32] use large numbers of untrimmed videos, each containing multiple actions, obtained either from YouTube (ActivityNet, THUMOS, MultiTHUMOS) or from crowd-sourced actors (Charades). The datasets also provide temporal (but not spatial) localization for each action of interest. AVA differs from them both in terms of content and annotation: we label a diverse collection of movies and provide spatio-temporal annotations for each subject performing an action in a large set of sampled frames.

A few datasets, such as CMU [20], MSR Actions [37], UCF Sports [29] and JHMDB [18] provide spatio-temporal annotations in each frame for short trimmed videos. The main differences with our AVA dataset are: the small number of actions ranging from 3 (MSR Actions) to at most 21 (JHMDB); the small number of video clips; and the fact that clips are trimmed. Furthermore, actions are complex (e.g., pole-vaulting) and not atomic as in AVA. For example, the UCF Sports dataset [29] consists of 10 sports actions, such as weight lifting, horse riding and diving. Recent extensions, such as UCF101 [33], DALY [35] and Hollywood2Tubes [23] evaluate spatio-temporal localization in untrimmed videos, which makes the task significantly harder and results in a performance drop. However, the action vocabulary is still restricted to a limited number of actions, at most 24, and actions are complex, which makes large-scale extension difficult. Moreover, they do not provide a dense coverage of all actions; a good example is BasketballDunk in UCF101 where only the player performing the dunk is annotated, whereas all the other players are not. These datasets are unrealistic – real-world applications require a continuous annotations of atomic actions, which can then be composed into higher-level events.

This paper addresses the main limitations of existing

datasets for spatio-temporal action recognition, which all consist of a small number of complex actions annotated in a small number of clips often in specific environments. Here, we depart from these drawbacks and annotate 80 atomic actions densely in 57.6k realistic movie clips resulting in 210k action labels.

The AVA dataset is also related to still image action recognition datasets [7, 9, 12]. Such datasets provide annotations for humans and their actions. Yet, still image action recognition datasets present two major drawbacks. First, the lack of motion information makes disambiguation in many cases difficult or impossible. We found that the context from surrounding video is essential in order to annotate the individual frames. Take for example the actions walking, standing and falling down. They all look very similar if only one frame is given for annotation. This necessity for motion information is also confirmed by our experiments. Second, modeling complex events as a *sequence* of individual atomic actions is not possible for still images. This is arguably out of scope here, but clearly required in many real-world applications, for which the AVA dataset does provide training data.

## 3. Data collection

The AVA Dataset generation pipeline consists of three stages: movie and segment selection, person bounding box annotation and action annotation.

### 3.1. Movie and segment selection

The raw video content of the AVA dataset comes from YouTube. We begin by assembling a list of top actors of various nationalities. For each name we issue a YouTube search query, retrieving up to 2000 results. We only include videos with the “film” or “television” topic annotation, a duration of over 30 minutes, at least 1 year since uploaded, and at least 1000 views. We further exclude black & white, low resolution, animated, cartoon, and gaming videos, as well as those containing mature content. Note that there is no explicit action distribution bias in this process, as the selection and filtering criteria does not include any action related keyword, nor does it run any automated action classifier on the video content.

Each movie contributes equally to the dataset, as we only label a sub-part ranging from the 15th to the 30th minute. We skip the beginning of the movie to avoid annotating titles or trailers. We choose a duration of 15 minutes so we are able to include more movies under a fixed annotation budget, and thus increase the diversity of our dataset.

Each 15-min clip is partitioned into 300 non-overlapping 3s movie segments. We choose 3s because the dataset focuses on atomic actions and our user studies confirm that 3s is a reasonably short length in which atomic actions can

be recognized. We choose to label 300 segments consecutively rather than randomly sampling segments from the whole movie to preserve *sequences of atomic actions* in a coherent temporal context.

Every human bounding box and its corresponding action labels are associated with a segment. Note that although annotators annotate only the middle frame, they take into account the information from the surrounding 3s segments. As stated in the introduction, annotating only one frame in a segment is a design choice to avoid ambiguous temporal annotation, which is not only error prone but also labor intensive. This choice also alleviates the shot boundary problem, as the action label and spatial localization are both well defined in the middle frame. Shots where the transition is too close to the middle frame are marked by annotators and removed from the dataset.

### 3.2. Bounding box annotation of subjects

We localize a person (subject) and his or her actions with a bounding box. When multiple subjects are present in a given middle frame, each subject is shown to the annotator separately for action annotation, and thus their action labels can be different.

Since bounding box annotation is manually intensive, we choose a hybrid approach. First, we generate an initial set of bounding boxes using the Faster-RCNN person detector [28]. We set the operating point to ensure high-precision. Annotators then annotate the remaining bounding boxes missed by our detector. Figure 3 shows the user interface for bounding box annotation. This hybrid approach ensures full bounding box recall which is essential for benchmarking, while minimizing the cost of manual annotation. This manual annotation retrieves only 5% more bounding boxes missed by our person detector. This demonstrates the excellent performance of our detector. Incorrect bounding boxes will be marked and removed by annotators in the next stage of action annotation.

### 3.3. Action annotation

The action labels are generated by crowd-sourced annotators using the interface shown in Figure 4. The left panel shows both the middle frame of the target segment (top) and the segment as a looping embedded video (bottom).

The bounding box overlaid on the middle frame specifies the subject whose action needs to be labeled. On the right are text boxes for entering up to 7 action labels. Actions are divided into pose/movement actions (denoted by the green box and required), person-object interactions (denoted by the yellow boxes and optional), and person-person interactions (denoted by the blue boxes and optional). For all three types, we provide a predefined list of actions from which to select. If none of the listed actions is suitable, a check box of “Action Other” is available to flag.

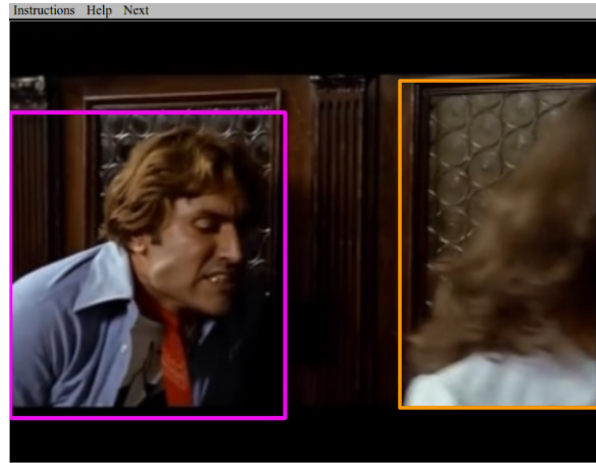


Figure 3. User interface for bounding box annotation. The purple box was generated by the person detector. The orange box (missed by the detector) was manually added by an annotator with a mouse.

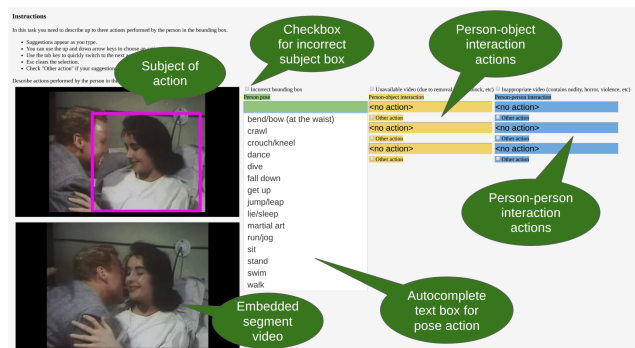


Figure 4. User interface for action annotation. Refer to Section 3.3 for details.

Finally, the annotator could flag segments containing blocked or inappropriate content, or incorrect bounding boxes. On average, annotators take 22 seconds to annotate a given video segment.

### 3.4. Training and test sets

Our training/test sets are split at the video level, so that all segments of one video appear only in one split. In detail, the 192 videos are split into 154 training and 38 test videos, resulting in 46.2k training segments and 11.4k test segments, roughly a 80%, 20% split. Each training/test segment is annotated by three annotators, where any action label annotated by two or more annotators are regarded as correct (to ensure accuracy of the test set). Action labels that are annotated by only one annotator are verified with more replications in the second round. See the analysis of annotation quality in Section 4.1. Annotators see segments in random order.

## 4. Characteristics of the AVA dataset

We start our analysis by discussing the nature and distribution of the data and showing that the annotation quality is high. We then explore the interesting action and temporal structure that makes this dataset truly unique. Finally, we discuss the characteristics that make the dataset challenging for the action detection task.

First, some examples to build intuition. Each example is presented as three frames from a clip: the middle frame with a bounding box around the person performing the action, one frame 0.5 seconds before the middle frame, and another 0.5 seconds after. The two additional frames provide context to visualize motion.

Figure 5 shows examples of different actions. We can see the huge variation in person bounding box height and position. The cinematography also differs, especially between genres, with different aspect ratios, techniques, and coloring. Shot boundaries may occur within a segment, such as the “fall down” example. However, recall that action labels only correspond to the middle frame, so they are still well defined. Some action instances can be identified from a single frame, such as “phone” or “brush teeth”. However many require within-frame context as well as temporal context, such as “take a photo”, “fall down” and “listen”. This makes the data especially interesting and complex.

Figure 6 shows three examples for the action “clink glass” (toast). Even within an action class the appearance varies widely with different person sizes and vastly different contexts. The recipient(s) of the toast may or may not be in the frame, and the glasses may be partially occluded. The temporal extent also varies - in the first the glasses are held up for a long time, in the second the action continues throughout, while in the third the action is not clear until the middle frame. The wide intra-class variety will allow us to learn features that identify the critical spatio-temporal parts of an action — such as touching glasses for “clink glass”.

Additional examples are in the supplemental material.

### 4.1. Annotation quality

To assess the consistency of the labels, three people annotated each bounding box in the test set, providing up to 21 raw labels in total. We define the *outlier ratio* as the number of raw labels that were provided by only one annotator (and are thus uncorroborated), divided by the total number of raw labels provided by all annotators. For example, for a segment with 5 total raw labels out of which 1 is only listed by one annotator, the outlier ratio is 0.2. A ratio of 0 means no uncorroborated labels, and 1 means complete disagreement. Figure 7 shows a histogram of the outlier ratios on the test set. The vast majority of ratios are very low, showing good inter-annotator consistency.

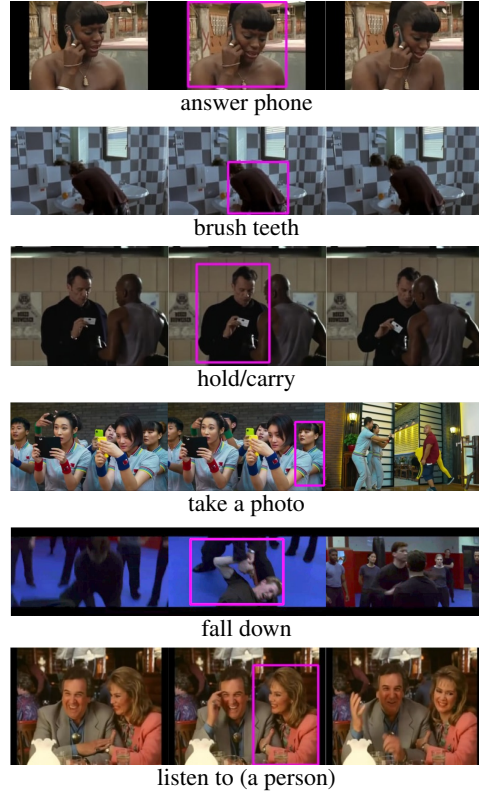


Figure 5. Examples from different label classes. The middle frame with the person bounding box is shown, along with frames at  $\pm 0.5$  seconds. Note the variety in person size and shape, cinematography and shot boundaries. Temporal and within-frame context are critical for the “take a photo”, “fall down” and “listen” examples.



Figure 6. Three examples of the label “clink glass” (toast). The middle frame with the person bounding box is shown, along with frames at  $\pm 0.5$  seconds. The appearance varies widely.

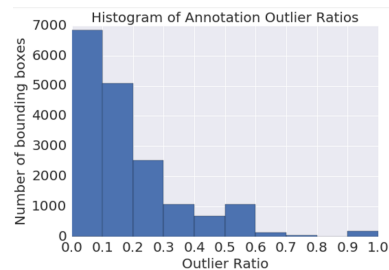


Figure 7. Histogram of the between-annotator label *outlier ratios* in the test set. Since the ratios are generally very low, we conclude that the annotators are consistent.

Pose Class	# Labels	Interaction Class	# Labels
stand	45790	talk to (self/a person)	29020
sit	30037	watch (a person)	25552
walk	12765	listen to (a person)	21557
bend/bow	2592	carry/hold (an object)	18381
lie/sleep	1897	ride	1344
dance	1406	answer phone	1025
run/jog	1146	watch (e.g., TV)	993
crouch/kneel	678	grab (a person)	936
martial art	624	smoke	860
get up	439	eat	828
jump/leap	151	fight/hit (a person)	707

Table 1. Most common pose and interaction labels in the AVA dataset. Interactions include both person-person and person-object. A full list is presented in the supplemental material.

	0	1	2	3+
# boxes w/ n poses	485	76505	-	-
# boxes w/ n person-object interactions	55718	18496	2635	141
# boxes w/ n person-person interactions	25179	38608	12854	349

Table 2. Counts of labels per person bounding box in the training set. “Action Other” labels are ignored. Almost all of the bounding boxes have a pose label in the predefined list, and the vast majority have at least one interaction as well. In total there are 76990 person bounding boxes with at least one label.

## 4.2. Action structure

With the quality of the annotations established, we next examine the data distribution. In total, there are 80 different action labels, in addition to “Action Other”, with 14 pose labels, 17 person-person interactions, and 49 person-object interactions. The most frequently occurring pose and interaction labels are shown in Table 1, with a full list in the supplemental material. Note the large variety of poses and interactions, from simple poses like “stand” to complex interactions like “watch (e.g., TV)”.

One important question is whether the lists of pose and interaction labels are sufficiently complete to describe the wide variety of movie content. The annotators assigned the label “Action Other” for poses or interactions that were not present in any label list (pose, person-person or person-object). Annotators never assigned “Action Other” twice to any one label category. Out of the 3 label categories per bounding box, the “Action Other” label was only used 1.0% of the time in the training set. This implies that the list is indeed sufficiently complete.

The data also show interesting structure, with multiple labels for the majority of person bounding boxes. Table 2 provides the frequencies of label counts per person bounding box. Recall there may be multiple people in a segment. “Action Other” labels are not counted. Almost all of the bounding boxes have a pose label from the list, which once again demonstrates that the label list has good coverage. In addition, the majority of bounding boxes have at least one interaction label. This demonstrates that the data are complex and layered despite the atomic nature of the actions.

Action 1	Action 2	NPMI
fight/hit (a person)	martial art	0.89
dig	shovel	0.79
play musical instrument	sing to (e.g. self/a person/a group)	0.66
climb (e.g. a mountain)	crawl	0.61
lift (a person)	play with kids	0.60
fight/hit (a person)	kick (a person)	0.59
chop	cut	0.58
row boat	sail boat	0.58
stand	watch (a person)	0.58
hug (a person)	kiss (a person)	0.58
dance	sit	-0.38
lie/sleep	stand	-0.42
sit	walk	-0.57

Table 3. The highest and lowest NPMI for pairs of labels for a single person in a given segment that occur together at least once in the training data.

Given the large number of examples with at least two labels, we can discover interesting patterns in the data that do not exist in other datasets. The Normalized Pointwise Mutual Information (NPMI) [8] is used in linguistics to represent the co-occurrence between two words, defined as:

$$\text{NPMI}(x, y) = \left( \ln \frac{p(x, y)}{p(x)p(y)} \right) / (-\ln p(x, y)) \quad (1)$$

Values intuitively fall in the range  $(-1, 1]$ , with  $\text{NPMI}(x, y) = -1$  (in the limit) for pairs of words that never co-occur,  $\text{NPMI}(x, y) = 0$  for independent pairs, and  $\text{NPMI}(x, y) = 1$  for pairs that always co-occur. Table 3 shows the label pairs with the top 9 and bottom 3 NPMI scores (for pairs that occur at least once).

We confirm expected patterns in the data, for example people frequently play instruments while singing. We can also see that martial arts often involve fighting, that people often lift (a person) while playing with kids, and that people hug while kissing. In this dataset people reassuringly do not sleep while standing, and they also do not sit while dancing. All of these pairwise co-occurrences of atomic actions will allow us to build up more complex actions in the future and to discover the compositional structure of complex activities.

## 4.3. Temporal structure

Another unique characteristic of the AVA dataset is the temporal structure. Recall that consecutive segments of three seconds are annotated, with skipped segments only if the bounding boxes were incorrect (rare) or there was no person in the middle frame. It is interesting to see how the actions evolve from segment to segment. Figure 8 shows the NPMI values for pairs of pose labels in consecutive three-second segments. The first pose is on the y-axis and the second is on the x-axis. Using the jet color map, an NPMI value of -1 (never co-occur) is dark blue, 0 (independent) is light green, and 1 (always co-occur) is dark red.

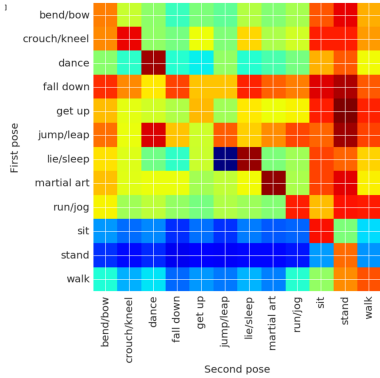


Figure 8. NPMI of pose label transitions between consecutive segments in the jet color map. Y-axis: Pose label in segment  $[t-3, t]$  seconds. X-axis: Pose label in segment  $[t, t+3]$  seconds. (Poses with less than 100 instances are excluded.)

As expected, transitions often occur between identical pose labels (on the diagonal) and from any label to the common labels “sit”, “stand” and “walk” (columns). Moreover, interesting common sense patterns arise. There are frequent transitions from “jump/leap” to “dance” and “crouch/kneel” to “bend/bow” (as someone stands up). Unlikely sequences can also be learned, for example “lie/sleep” is rarely followed by “jump/leap”.

The transitions between atomic actions with high NPMI scores (despite the relatively coarse temporal sampling) provide excellent training data for building more complex actions and activities with temporal structure.

#### 4.4. Data complexity

The first contributor to complexity is a wide variety of labels and instances. The above analysis discussed the long label lists and the wide distribution of class sizes. The second contributor to complexity is appearance variety. The bounding box size distribution illustrates this. A large portion of people take up the full height of the frame. However there are still many boxes with smaller sizes. The variability can be explained by both zoom level as well as pose. For example, boxes with the label “enter” show the typical pedestrian aspect ratio of 1:2 with average widths of 30% of the image width, and an average heights of 72%. On the other hand, boxes labeled “lie/sleep” are closer to square, with average widths of 58% and heights of 67%. The box widths are quite widely distributed, showing the variety of poses people must undertake to execute the labeled actions.

The breadth of poses, interactions, action co-occurrences, and human pose variability make this a particularly challenging dataset.

## 5. Experiments

### 5.1. Experimental setup

As shown in Table 1 and the supplemental material, the label distribution in the AVA dataset follows roughly Zipf’s law. Since evaluation on very small test set could be unreliable, we only use those classes that have at least 25 test instances to benchmark action localization performance. Our benchmark set consists of 44 action classes that meet the requirement, and they have a minimal number of 90 training instances per class. We randomly select 10% of training data as validation set and use them to tune model parameters.

To demonstrate the competitiveness of our baseline methods, we also apply them to the JHMDB dataset [18] and compare the results against the previous state-of-the-art. We use the official split1 provided by the dataset for training and validation.

One key difference between AVA and JHMDB (as well as many other action datasets) is that action labels in AVA are not mutually exclusive, i.e., multiple labels can be assigned to one bounding box. To address this, we replace the common softmax loss function by the sum of per-class sigmoid losses, so labels do not compete with each other during optimization. We keep the softmax loss on JHMDB as it is the default loss used by previous methods on this dataset. The rest of the baseline model settings are the same for the two datasets.

We follow the protocol used by the PASCAL VOC challenge [9] and report the mean average precision (mAP) over all action classes using an intersection-over-union threshold of 0.5. This metric is also commonly used to evaluate action localization.

### 5.2. Baseline approach

Current leading methods for spatio-temporal action recognition are all based on extensions of R-CNN [10] on videos [11, 30, 34, 35]. We use Faster R-CNN [28] and follow the end-to-end training procedure proposed by Peng & Schmid [26], except replacing the VGG network by the 101-layer ResNet [13] which has higher performance on image classification tasks. Our Faster R-CNN is implemented in TensorFlow.

To combine RGB with flow results, we first run the region proposal networks (RPN) using RGB and flow models independently. Then, we take top 100 scoring RPN proposals from the output of each network, and perform non-max suppression on the union. Once these proposals are obtained, we run the RGB and flow models in the “Fast R-CNN” mode, and take the average of classification scores for each bounding box proposal.

**RGB and optical flow extraction.** To extract optical flow, we estimate the camera motion information and use

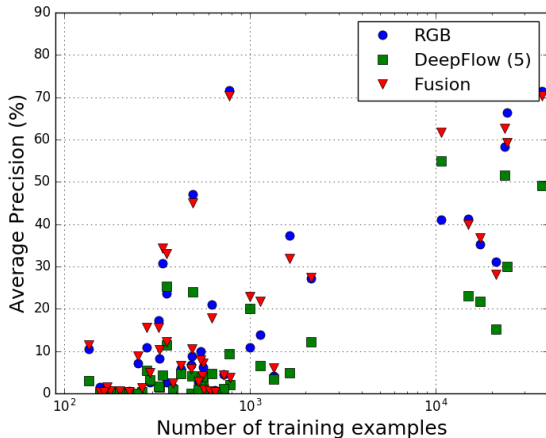


Figure 9. In this scatter-plot the points correspond to the average precision for each of the 44 action classes in the benchmark set. For any such point, the x-coordinate is the number of training examples for that action, and the y-coordinate is the average precision. The colors code for the three different models based on using RGB alone, optical flow alone, and their fusion.

the compensated flow fields. The  $u$  and  $v$  values from the flow fields are truncated to  $[-20, 20]$ , then quantized to  $[0, 255]$  to be stored as JPEG images, where the 3rd channel contains all zeros. We employ two methods: the dense optical flow estimation method TVL-1 [27], and a CNN-based iterative Deep Flow model which is a variant of the FlowNet-ss network [17]. It has 11M parameters, takes 360ms per frame on a CPU, and achieves an EPE of 4.4 on Sintel final [5].

We also experiment with single flow vs. a stack of 5 consecutive flows, and expect the latter to perform better as it captures more temporal information.

Images and encoded optical flows are resized to 256 by 340 pixels for JHMDB and 600 by 800 pixels for AVA. We use a higher resolution for AVA because the dataset contains a larger portion of small bounding boxes.

**Model parameters and initialization.** We train the Faster R-CNN action detector asynchronously using the momentum optimizer with momentum set to 0.9. The batch size is 64 for the RPN and 256 for the box classifier. Hyperparameters are mostly fixed to default values used in [15] for the COCO object detection task. The only exceptions are the training steps and the learning rates which are selected using the validation set. Our models are trained at the learning rate of  $2e-4$  for the initial 600K steps, and  $2e-5$  for the next 200K steps.

We initialize model weights using the open-source ResNet-101 checkpoint from [13]. For optical flow model initialization, we take the weights from the first *conv1* layer of ResNet-101 for the first two input channels, and duplicate them to match dimensions of flow inputs.

	JHMDB	AVA
Two-stream [26]	56.6%	N/A
Multi-region [26]	58.5%	N/A
RGB	52.0%	17.1%
TVL-1 (1)	25.2%	6.7%
TVL-1 (5)	42.3%	8.5%
Deep Flow (1)	29.9%	7.3%
Deep Flow (5)	48.4%	9.3%
RGB + TVL-1 (5)	58.5%	18.1%
RGB + Deep Flow (5)	62.0%	18.4%

Table 4. Mean average precision at IOU threshold of 0.5 for JHMDB split1 and AVA benchmark.

	Large	Medium	Small
RGB	17.3%	12.9%	2.7%
TVL-1 (1)	7.0%	0.9%	0.9%
TVL-1 (5)	8.8%	1.7%	1.7%
Deep Flow (1)	7.5%	0.7%	0.9%
Deep Flow (5)	9.7%	0.9%	0.9%
RGB + TVL-1 (5)	18.5%	14.3%	2.8%
RGB + Deep Flow (5)	18.8%	14.0%	2.7%

Table 5. Mean average precision at IOU threshold of 0.5 on AVA benchmark, separated by box sizes. Boxes smaller than  $42 \times 42$  pixels are small, and larger than  $96 \times 96$  pixels are large.

### 5.3. Experimental results

Table 4 summarizes our baseline performance on the JHMDB and AVA datasets. Our baseline method outperforms the previous state of the art on JHMDB [26] by a significant margin (62.0% vs. 58.5%). Nevertheless, its performance on the AVA benchmark dataset is significantly lower than on JHMDB. This result demonstrates the difficulty of our dataset, and opens up opportunities to explore new, maybe even drastically different solutions for action localization.

On both datasets, the RGB based model achieves the best standalone performance, and fusion with optical flow models gives better performance. We can also see that using Deep Flow extracted flows and stacking multiple flows are both helpful for JHMDB as well as AVA.

Table 5 breaks down the performance by bounding box sizes. The results align with the discovery from the COCO detection challenge, i.e., small bounding boxes have the lowest performance because they are hardest to localize and classify. Figure 9 shows individual class APs with their training example size. As we can see, there are rare classes which are “easy” and that having lots of data does not necessarily mean high mAP.

## 6. Conclusion

This paper introduces the AVA dataset and shows that current state-of-the-art methods, which work well on previous datasets, do not perform well on AVA. This moti-

vates the need for developing new approaches. The AVA dataset enables measuring performance and progress in realistic scenarios.

Future work includes modeling more complex actions and activities based on our atomic actions (see analysis in section 4.3). Our present day visual classification technology may enable us to classify events such as “eating in a restaurant” at the coarse scene/video level, but only models based on AVA’s fine spatio-temporal granularity offer us the hope of understanding at the level of an individual agent’s actions. These are essential steps towards imbuing computers with “social visual intelligence” – understanding what humans are doing, what might they do next, and what they are trying to achieve.

## 7. Acknowledgement

We thank Irfan Essa and Abhinav Gupta for discussions and comments about this work.

## References

- [1] S. Abu-El-Haija, N. Kothari, J. Lee, P. Natsev, G. Toderici, B. Varadarajan, and S. Vijayanarasimhan. YouTube-8M: A large-scale video classification benchmark. *arXiv:1609.08675*, 2016. 3
- [2] D. Arijon. *Grammar of the film language*. Silman-James Press, 1991. 2
- [3] R. Barker and H. Wright. *Midwest and its children: The psychological ecology of an American town*. Row, Peterson and Company, 1954. 2
- [4] M. Blank, L. Gorelick, E. Shechtman, M. Irani, and R. Basri. Actions as space-time shapes. In *ICCV*, 2005. 3
- [5] D. J. Butler, J. Wulff, G. B. Stanley, and M. J. Black. A naturalistic open source movie for optical flow evaluation. In *ECCV*, 2012. 8
- [6] F. Caba Heilbron, V. Escorcia, B. Ghanem, and J. C. Niebles. ActivityNet: A large-scale video benchmark for human activity understanding. In *CVPR*, 2015. 3
- [7] Y.-W. Chao, Z. Wang, Y. He, J. Wang, and J. Deng. HICO: A benchmark for recognizing human-object interactions in images. In *ICCV*, 2015. 3
- [8] K.-W. Church and P. Hanks. Word association norms, mutual information, and lexicoraphy. *Computational Linguistics*, 16(1), 1990. 6
- [9] M. Everingham, S. M. A. Eslami, L. Van Gool, C. K. I. Williams, J. Winn, and A. Zisserman. The PASCAL visual object classes challenge: A retrospective. *IJCV*, 111(1), 2015. 3, 7
- [10] R. Girshick, J. Donahue, T. Darrell, and J. Malik. Rich feature hierarchies for accurate object detection and semantic segmentation. In *CVPR*, 2014. 7
- [11] G. Gkioxari and J. Malik. Finding action tubes. In *CVPR*, 2015. 7
- [12] S. Gupta and J. Malik. Visual semantic role labeling. *CoRR*, abs/1505.04474, 2015. 3
- [13] K. He, X. Zhang, S. Ren, and J. Sun. Deep residual learning for image recognition. In *CVPR*, 2016. 7, 8
- [14] F. Heider and M. Simmel. An experimental study of apparent behavior. *The Am. J PSYCH*, 57(2), 1944. 2
- [15] J. Huang, V. Rathod, C. Sun, M. Zhu, A. Korattikara, A. Fathi, I. Fischer, Z. Wojna, Y. Song, S. Guadararama, and K. Murphy. Speed/accuracy trade-offs for modern convolutional object detectors. In *CVPR*, 2017. 8
- [16] H. Idrees, A. R. Zamir, Y. Jiang, A. Gorban, I. Laptev, R. Sukthankar, and M. Shah. The THUMOS challenge on action recognition for videos “in the wild”. *CVIU*, 2017. 2, 3
- [17] E. Ilg, N. Mayer, T. Saikia, M. Keuper, A. Dosovitskiy, and T. Brox. FlowNet 2.0: Evolution of optical flow estimation with deep networks. *arXiv:1612.01925*, 2016. 8
- [18] H. Jhuang, J. Gall, S. Zuffi, C. Schmid, and M. Black. Towards understanding action recognition. In *ICCV*, 2013. 3, 7
- [19] A. Karpathy, G. Toderici, S. Shetty, T. Leung, R. Sukthankar, and L. Fei-Fei. Large-scale video classification with convolutional neural networks. In *CVPR*, 2014. 3
- [20] Y. Ke, R. Sukthankar, and M. Hebert. Efficient visual event detection using volumetric features. In *ICCV*, 2005. 3
- [21] H. Kuehne, H. Jhuang, E. Garrote, T. Poggio, and T. Serre. HMDB: A large video database for human motion recognition. In *ICCV*, 2011. 3
- [22] M. Marszalek, I. Laptev, and C. Schmid. Actions in context. In *CVPR*, 2009. 3
- [23] P. Mettes, J. van Gemert, and C. Snoek. Spot On: Action localization from pointly-supervised proposals. In *ECCV*, 2016. 3
- [24] D. Newtonson. Attribution and the unit of perception in ongoing behavior. *Journal of Personality and Social Psychology*, 28(1), 1973. 2
- [25] P. Over, G. Awad, M. Michel, J. Fiscus, G. Sanders, W. Kraaij, A. Smeaton, and G. Quénot. TRECVID 2014 – an overview of the goals, tasks, data, evaluation mechanisms and metrics, 2014. 3
- [26] X. Peng and C. Schmid. Multi-region two-stream r-cnn for action detection. In *Proc. ECCV*, pages 744–759. Springer, 2016. 7, 8

- [27] J. S. Pérez, E. Meinhardt-Llopis, and G. Facciolo. TV-L1 optical flow estimation. *Image Processing On Line*, 2013:137–150, 2013. 8
- [28] S. Ren, K. He, R. Girshick, and J. Sun. Faster R-CNN: Towards real-time object detection with region proposal networks. In *NIPS*, pages 91–99, 2015. 4, 7
- [29] M. Rodriguez, J. Ahmed, and M. Shah. Action MACH: a spatio-temporal maximum average correlation height filter for action recognition. In *CVPR*, 2008. 3
- [30] S. Saha, G. Singh, M. Sapienza, P. Torr, and F. Cuzzolin. Deep learning for detecting multiple space-time action tubes in videos. In *BMVC*, 2016. 7
- [31] C. Schuldt, I. Laptev, and B. Caputo. Recognizing human actions: a local SVM approach. In *ICPR*, 2004. 3
- [32] G. Sigurdsson, G. Varol, X. Wang, A. Farhadi, I. Laptev, and A. Gupta. Hollywood in homes: Crowdsourcing data collection for activity understanding. In *ECCV*, 2016. 3
- [33] K. Soomro, A. Zamir, and M. Shah. UCF101: A dataset of 101 human actions classes from videos in the wild. Technical Report CRCV-TR-12-01, University of Central Florida, 2012. 3
- [34] P. Weinzaepfel, Z. Harchaoui, and C. Schmid. Learning to track for spatio-temporal action localization. In *ICCV*, 2015. 7
- [35] P. Weinzaepfel, X. Martin, and C. Schmid. Towards weakly-supervised action localization. *arXiv:1605.05197*, 2016. 3, 7
- [36] S. Yeung, O. Russakovsky, N. Jin, M. Andriluka, G. Mori, and L. Fei-Fei. Every moment counts: Dense detailed labeling of actions in complex videos. *arXiv:1507.05738*, 2015. 3
- [37] J. Yuan, Z. Liu, and Y. Wu. Discriminative subvolume search for efficient action detection. In *CVPR*, 2009. 3
- [38] J. Zacks and B. Tversky. Event structure in perception and conception. *Psychol. Bull.*, 127(1), 2001. 2
- [39] J. Zacks, B. Tversky, and G. Iyer. Perceiving, remembering and communicating structure in events. *J. Exp. Psychol.-Gen.*, 130(1), 2001. 2

## Appendix

In the appendix, we present additional quantitative information and examples for our AVA dataset as well as for our action detection approach.

Table 6 and 7 present the number of instances for each class of the AVA dataset. We observe a significant class imbalance to be expected in real-world data [c.f. Zipf’s Law]. As stated in the paper, we select a subset of these classes (without asterisks) for our benchmarking experiment, in order to have a sufficient number of test examples. Note that we consider the presence of the “rare” classes as an opportunity for approaches to learn from a few training examples.

Figures 10–13 show additional examples for several action labels in the AVA dataset. For each example, we also display the neighboring frames at  $\pm 0.5$  seconds in order to provide temporal context. We recall that our annotators use the surrounding 3 seconds to decide on the label. These examples demonstrate the large diversity of our dataset due to the variety in person size and shape, cinematography and shot boundaries.

Figure 14 shows per-class action detection results for the AVA benchmark dataset. We can observe that flow outperforms RGB for classes with significant motion such as “get up”, “hit (a person)”, “run/jog”, and “walk”. Fusion of RGB and flow outperforms the individual results.

Figure 15 visualizes examples of our action detection approach with fusion of RGB and flow. We show examples with high confidence, i.e., above a threshold of 0.8. In case of multiple labels for a human, we display the average box, if  $\text{IoU} > 0.7$ .

Pose	#	Person-Person Interaction	#
stand	45790	talk to (e.g. self/person)	29020
sit	30037	watch (a person)	25552
walk	12765	listen to (a person)	21557
bend/bow (at the waist)	2592	grab (a person)	936
lie/sleep	1897	fight/hit (a person)	707
dance	1406	sing to (e.g. self/person)	702
run/jog	1146	hug (a person)	667
crouch/kneel	678	give/serve (an object) to (a person)	473
martial art	624	hand clap	470
get up	439	kiss (a person)	370
jump/leap*	151	take (an object) from (a person)	257
fall down	114	hand wave	241
crawl*	61	lift (a person)	201
swim*	32	hand shake	179
		push (another person)*	122
		play with kids*	70
		kick (a person)*	13

Table 6. Number of instances for pose (left) and person-person (right) action labels in the AVA dataset, sorted in decreasing order. Labels marked by asterisks are not included in the benchmark dataset.

Person-Object Interaction	#	Person-Object Interaction	#
carry/hold (an object)	18381	enter*	58
ride (e.g. bike/car/horse)	1344	climb (e.g. a mountain)*	57
answer phone	1025	take a photo*	57
watch (e.g. TV)	993	push (an object)*	56
smoke	860	play with pets*	52
eat	828	point to (an object)*	45
read	698	cut*	43
touch (an object)	670	shoot*	41
open (e.g. window/car door)	594	dig*	40
play musical instrument	545	press*	38
lift/pick up	452	play board game*	35
drink	410	cook*	31
drive (e.g. car/truck)	383	clink glass*	30
put down	369	fishing*	27
write	340	paint*	25
close (e.g. door/box)	334	row boat*	23
listen (e.g. to music)	290	extract*	17
catch (an object)	281	chop*	15
pull (an object)	193	stir*	15
dress/put on clothing*	130	brush teeth*	14
text on/look at a cellphone*	115	kick (an object)*	10
throw*	99	exit*	9
sail boat*	96	turn (e.g. a screwdriver)*	8
work on a computer*	94	shovel*	2
hit (an object)*	67		

Table 7. Number of instances for person-object interactions in the AVA dataset, sorted in decreasing order. Labels marked by asterisks are not included in the benchmark.



Figure 10. Examples from different label classes. The middle frame with the person bounding box is shown, along with frames at  $\pm 0.5$  seconds. Notice the variety in person size and shape, cinematography and shot boundaries.



Figure 11. Examples from different label classes. The middle frame with the person bounding box is shown, along with frames at  $\pm 0.5$  seconds. Notice the variety in person size and shape, cinematography and shot boundaries.



Figure 12. Examples from different label classes. The middle frame with the person bounding box is shown, along with frames at  $\pm 0.5$  seconds. Notice the variety in person size and shape, cinematography and shot boundaries.

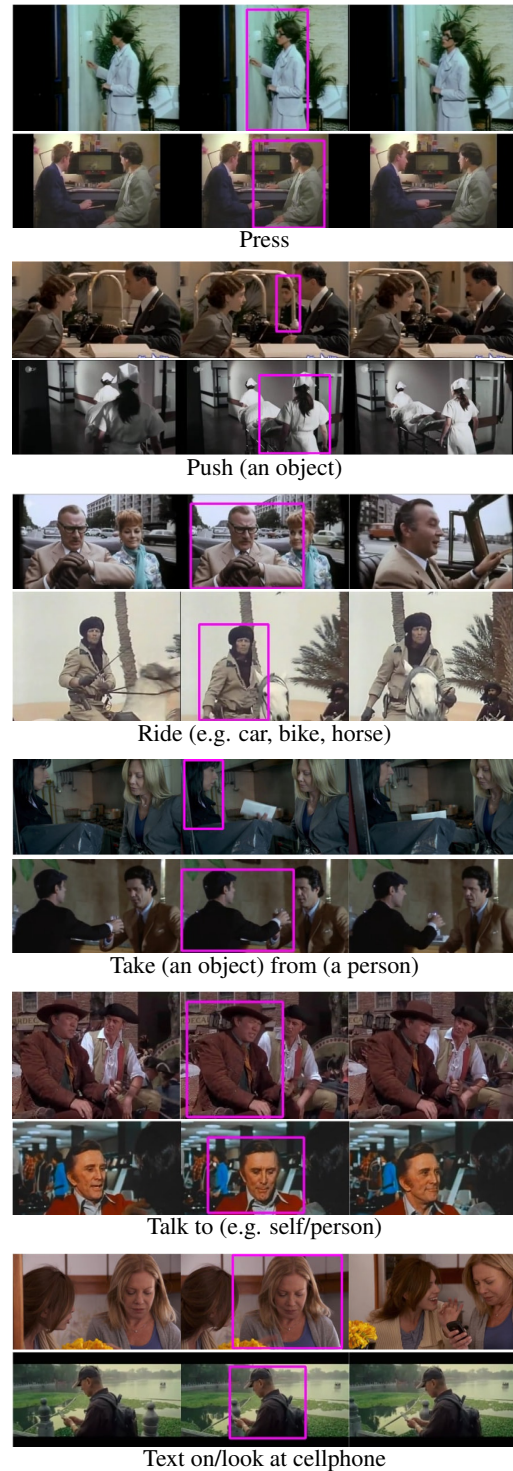


Figure 13. Examples from different label classes. The middle frame with the person bounding box is shown, along with frames at  $\pm 0.5$  seconds. Notice the variety in person size and shape, cinematography and shot boundaries.

Average Precision @ IOU > 0.5

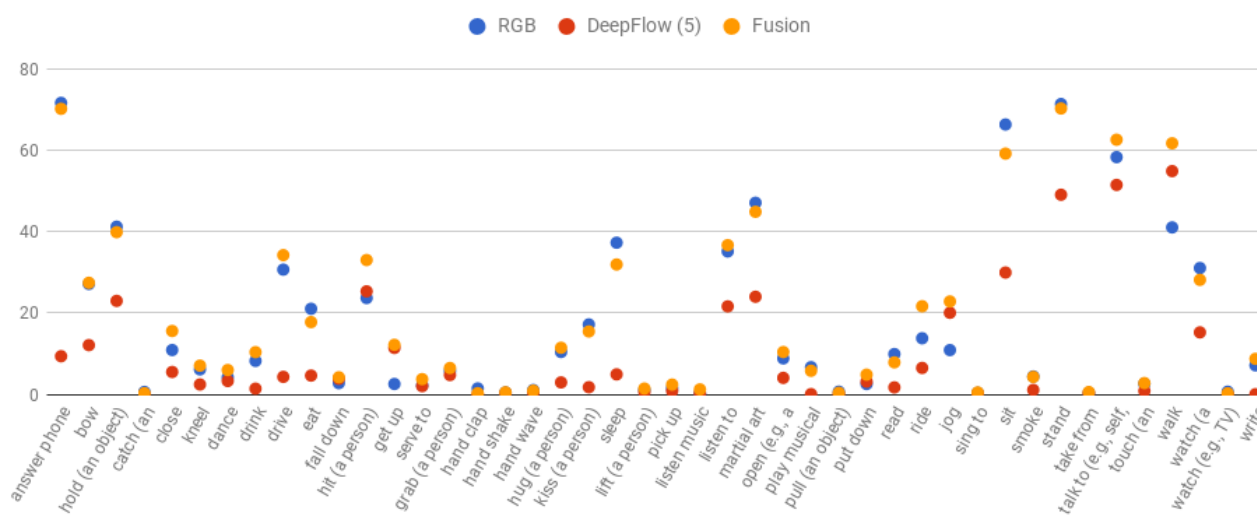


Figure 14. Average Precision at IoU threshold of 50% for the 44 action class in our AVA benchmark dataset (with more than 25 test examples). DeepFlow outperforms RGB for action classes with significant motion such as *get up*, *hit*, *jog*, and *walk*. Fusion of the two streams generally improves the performance.

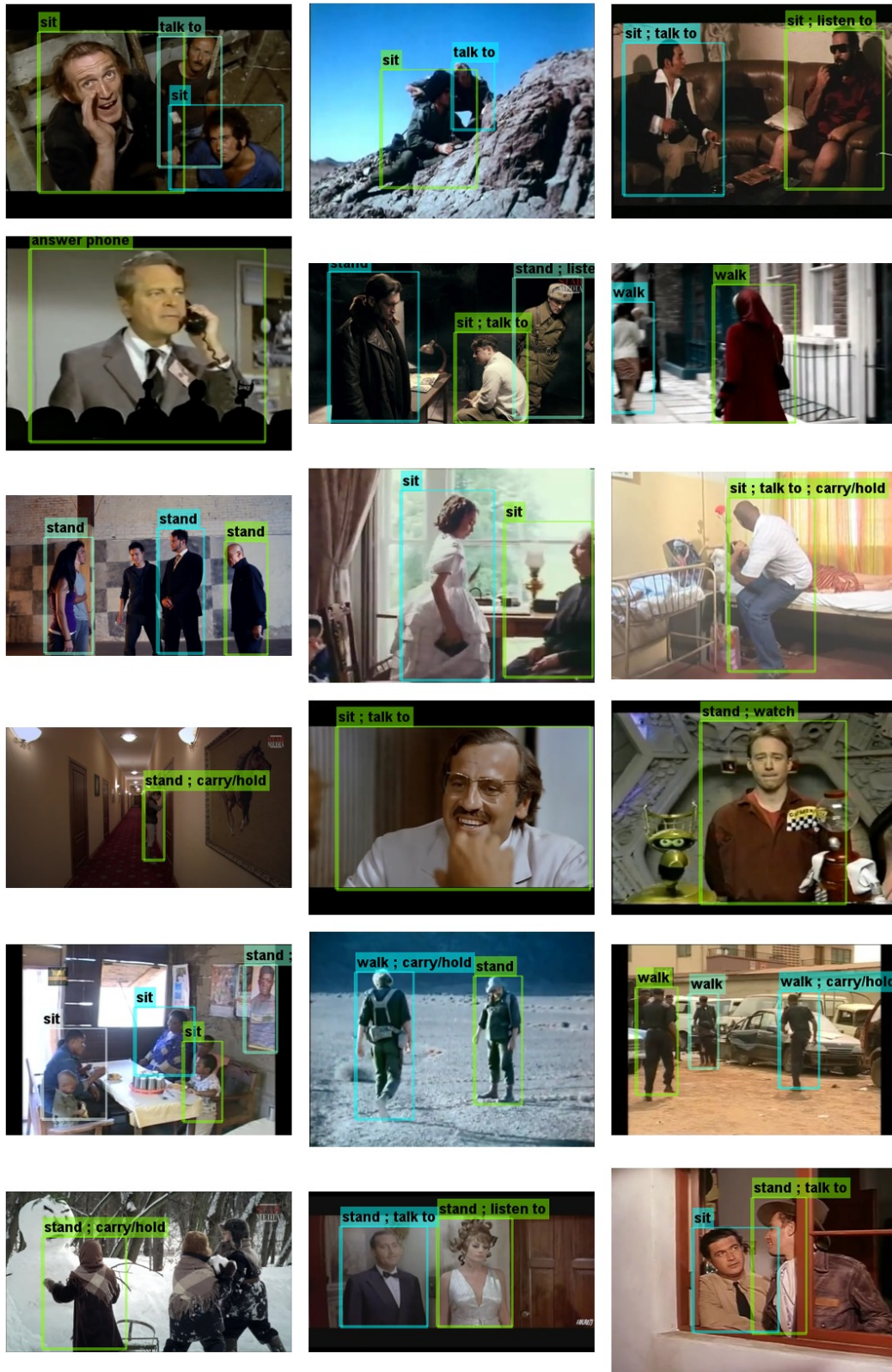


Figure 15. Example results of our action detection approach with fusion of RGB and flow with a confidence score above 0.8. In case of multiple labels of a human, we display the average box, if IoU > 0.7. Different actors are identified with different colors.